# Drag coefficient of solid micro-sphere between parallel plates

**S A Poniaev[1,2], K K Soboleva[3], A I Sobolev[3], V V Dudelev[4], G S Sokolovskii[1]**

[1]Ioffe Institute, St.Petersburg, Russia

[2]Mozhaiskiy Military Space Academy, St.Petersburg, Russia

[3]Peter the Great St.Petersburg Polytechnic University, St.Petersburg, Russia

[4]ITMO University, St.Petersburg, Russia

Email: serguei.poniaev@mail.ioffe.ru

**Abstract.** We present results of numerical simulation of the drag force acting on a spherical micro-particle in a two-wall channel formed by parallel plates. Dependence of the drag force on the distance between the particle and the channel wall is studied for different channel heights. We show the drag force in a two-wall channel with the height of the order of the particle diameter to be significantly higher than that in the single-wall counterpart.

## 1. Introduction

At present investigations of non-contact manipulation of micrometer-sized objects attract a considerable attention of researchers. The method is based on the optical trapping of the micrometer-sized particles as suggested in the 1970s [1]. The initial idea led to the development of a single-beam gradient force optical traps or "optical tweezers" capable of manipulation with the particles sized 1s-10s micrometers. Nowadays optical tweezers are widely used in many areas of physics and biology [2-5]. One of the emerging and fast-developing applications of the optical tweezers is lab-on-a-chip devices for manipulation and analysis of biological specimens. In such a prospective devices, micrometer-sized particles may be trapped and manipulated by the beams of semiconductor lasers which are the most compact and effective light emitters. However, application of the laser diodes to the optical trapping is hindered by the low spatial quality of their beams [6] resulting in the high beam propagation parameter $M^2$. The impact of the high $M^2$ values on the optical trap must be taken into account even for super-focused [7], non-diverging [8-10], and self-focused [11] laser diode beams and results in considerable reduction of the trapping force. On the other hand, if a particle is located in a wall-bounded flow, the particle drag coefficient can change in a wide range and the drag force can exceed the trapping force that leads to loss of trapping and escape of the particle from the laser beam. Therefore, it is highly important to have a proper understanding of the drag force acting on a micrometer-sized particle being moved near a wall of a channel.

The spherical solid particle motion in an unbounded flow and near a wall in a single-wall channel configuration has been extensively studied. These problems were considered in many publications,

both experimental and theoretical, where the hydrodynamic forces acting on a spherical particle were investigated [12-14] and where several sphere drag coefficient approximations were suggested [15].

However, there are few investigations of the channel configuration with two walls in the form of parallel plates, and only a small part of them are experimental. For example, the experimental data on the drag force given in [16] allow one to compare the numerical simulation and experimental results only for the centre line between two parallel plates. There are no data for other areas of the channel.

## 2. Numerical model

Figure 1 shows schematically a sphere in a channel and characteristics of the computational zone. The sphere with diameter D moves with velocity $V_s$ parallel to the channel wall. The channel height is H and the distance between the channel wall and the sphere surface is d.

The flow near the sphere moving with velocity $V_s$ in a quiescent fluid can be described in the dimensionless form as

$$\nabla \cdot U = 0$$
$$\frac{\partial U}{\partial t} + (U \cdot \nabla)U = -\nabla p + \frac{1}{\mathrm{Re}}\nabla^2 U \quad (1)$$

where U is the dimensionless flow velocity, p is the dimensionless pressure, and the Reynolds number (the ratio of the inertial to viscous forces) is $\mathrm{Re} = V_s D/\nu$. The coordinates, velocity, time, and pressure in the governing equations are normalized by using the characteristic values D, $V_s$, $D/V_s$, $\rho V_s^2$, respectively, where ρ is the fluid density, and ν is the fluid kinematic viscosity. When the sphere moves in a fluid, the drag force $F_D$ acting on the sphere arises. This force is due to the pressure and viscous effects. The drag coefficient $C_D$ can be expressed as the ratio between the drag force, unit kinetic energy, and sphere cross-section area $C_D = \frac{2F_D}{\rho V_s^2 (1/4\pi D^2)}$.

To carry out numerical simulation, a reference frame was attached to the sphere. In this case the boundary conditions on the channel walls and inlet (the right-hand side of the computational domain) are given by u = -U and v = w = 0, the boundary conditions on the outlet (left-hand side of the computational domain) are $\frac{\partial U}{\partial x} = 0$, and the boundary conditions on the sphere surface are u = v = w = 0. In this paper a motion of micro-particles in a small-size channel is considered, so the typical Reynolds number is $10^{-3}$.

A modified incompressible solver based on the OpenFOAM package [17] in a full 3D zone with a spherical particle was used for the numerical simulation. In the package, a finite-volume method was employed. For simulation, second-order spatial schemes with a minimal dissipation were chosen.

A grid and domain size independence study was performed by using an unbounded flow and single-wall channel flow as a benchmark for validation. The mesh convergence study was carried out by the 2x mesh refinement till the difference in the drag coefficient between the calculated and analytical values became as low as 1%.

There is a simple relation between the drag coefficient and Reynolds number for an unbounded flow, i.e., the flow without any walls [18]

$$C_{Dfree} = \frac{24}{\mathrm{Re}}(1 + 0.15\mathrm{Re}^{0.687}) \quad (2)$$

In the text below, $C_{Dfree}$ will be used as a characteristic value for the drag coefficient normalization.

Table 1 shows results of the grid and domain size independence study for a unbounded flow configuration. The mesh size is denoted by MxN, where M is the number of cells in the radial direction and N is the number of cells around the central cross-section of the sphere, the domain size $D_d$ is normalized by using D as a characteristic value. Figure 2 shows an example of the mesh and computational region in case of unbounded flow. All simulations were made for $\mathrm{Re}=10^{-3}$.

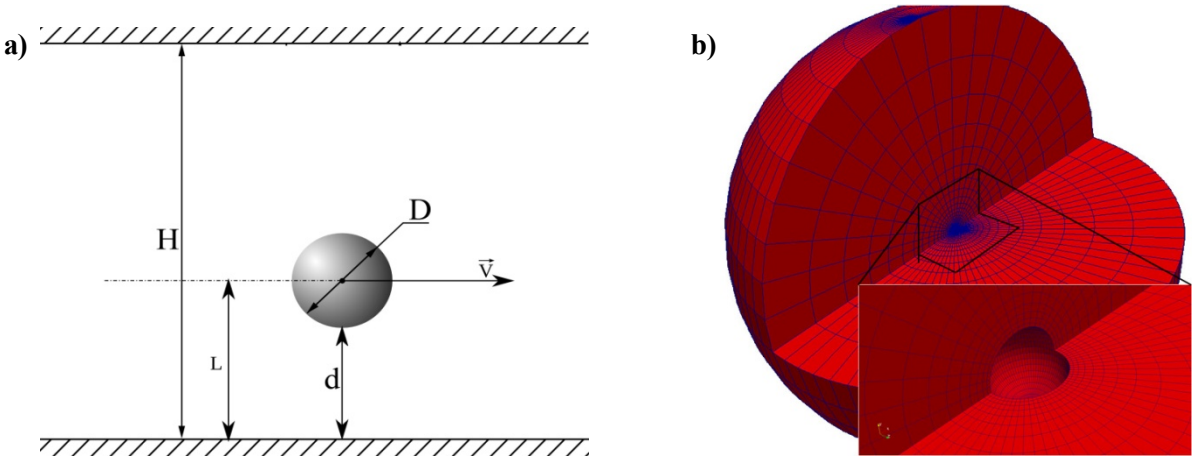


**Figure 1.** Schematic of sphere motion in the channel (a) and characteristics of the computational domain and mesh near the sphere (b).

**Table 1.** Drag coefficients for different computational domain and mesh sizes.

| No. | Mesh size RxS | Domain size, $D_d/D$ | $C_{D\_ns}$ numerical simulation | $C_{Dfree}$ calculated from (2) | $\Delta = (C_{D\_ns}-C_{Dfree})/C_{D\_ns}*100$ % |
|---|---|---|---|---|---|
| 1 | 10x20 | 10 | 24649 | 24031 | 2.5 |
| 2 | 20x40 | 10 | 25283 | 24031 | 5.0 |
| 3 | 10x20 | 20 | 24700 | 24031 | 2.7 |
| 4 | 20x20 | 20 | 24350 | 24031 | 1.3 |
| 5 | 20x40 | 20 | 24190 | 24031 | 0.7 |

Thus, the domain size equal to 20 sphere diameters and the mesh size equal to 20x40 was chosen for the numerical simulation.

Changes in the drag coefficient in a single-wall channel configuration have been considered by many authors. For the case when a sphere nearly touches the channel wall, i.e. $d \to 0$, a lubrication theory [19] gives an approximation for the drag coefficient as:

$$C_D = \frac{24}{\mathrm{Re}}\left(0.9588 - \frac{8}{15} ln\left(2\frac{d}{D}\right)\right) \tag{3}$$

So it is evident that there is logarithmic singularity when the sphere approaches the channel wall. The approximation valid for any values of d was suggested in [15]:

$$\begin{gathered} C_D = C_{D0}\left(1 + \alpha \mathrm{Re}^{\beta}\right) \\ C_{D0} = \frac{24}{\mathrm{Re}}\left(1.028 - \frac{0.07}{(1+4(d/D)^2)} - \frac{8}{15} ln\left(270\frac{(d/D)}{(135+256(d/D))}\right)\right) \\ \alpha = 0.15\left(1 - exp\left(-\sqrt{(d/D)}\right)\right) \\ \beta = 0.687 + 0.313exp\left(-2\sqrt{(d/D)}\right) \end{gathered} \tag{4}$$

As the authors of [15] stated, the above expression reduces to correct limits for small and large d. Figure 3 shows a normalized drag coefficient (the characteristic value for the normalization is the drag coefficient for an unbounded flow) obtained in the numerical simulation for different dimensionless distances (d/D) from the sphere. Approximations (3) and (4) are also plotted in this figure.

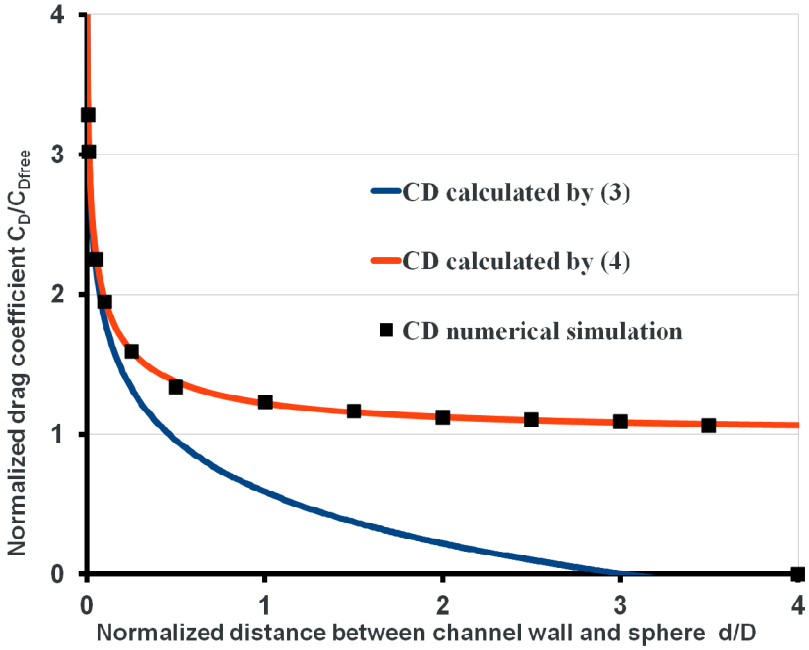


**Figure 3.** Variation in normalized drag coefficient for different normalized distances from the wall.

It is clearly seen that approximation (3) gives wrong results for large d/D values, but it is in a very good agreement for d → 0 as expected. Approximation (4) shows reasonable values in the entire region of simulation. The data obtained in the numerical simulation are in very good agreement with approximation (4), which confirms the correctness of the choice of the computational zone and mesh sizes.

## 3. Results and discussion

The main goal of our study was to perform numerical simulation for a solid sphere in a two-wall channel configuration, i.e. between parallel plates. In the course of numerical simulation the channel height was varied from 1.1 to 10 sphere diameters. To compare the results obtained in our numerical simulation with the experiment, we used the experimental data for the centre line of the two-wall channel [16]. In [16], the experimental data were approximated by a $14^{th}$ degree polynomial. So it is possible to calculate the drag coefficient at the centre line for channels of different heights.

Figure 4 shows the data for the normalized drag coefficient for the channels with the heights equal to 1.1, 2, 5, and 10 sphere diameters. In these figures approximation (4) that presents the drag coefficient for a single-wall configuration is also plotted.

It is clearly seen that the computed results are higher than those approximated for the channel with H/D <5 in the entire range of distances between the wall and sphere surface. The computed results for the channel with H/D=10 are in good agreement with the single-wall approximation. The simulation results for the channel with H/D=5 are slightly higher than those approximated for the single-wall

case. There is also an excellent agreement between the results of our numerical simulation and approximation of the experimental data reported in [16] for the center line of the channel.

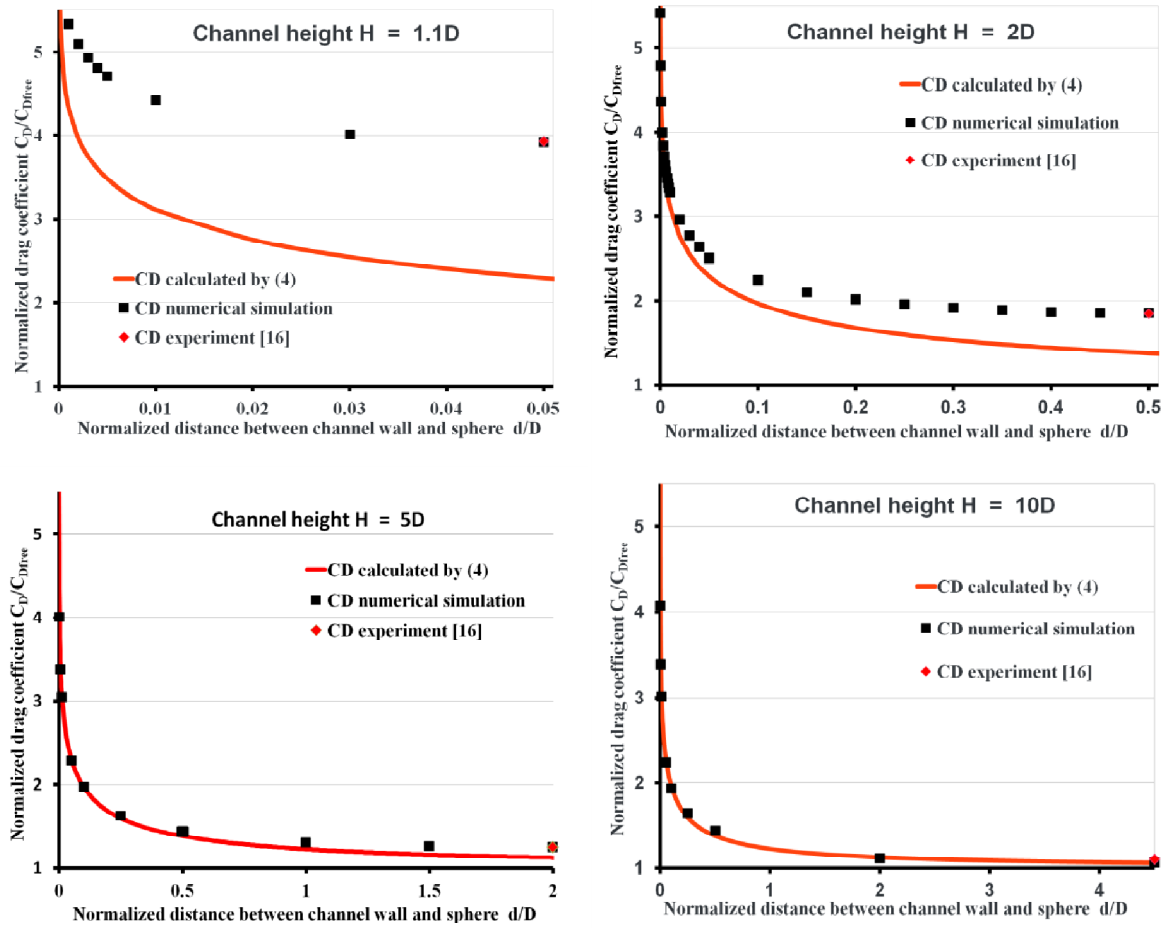


**Figure 4.** Normalized drag coefficient vs normalized distance between the sphere and wall for different channel heights.

Our results clearly show that the sphere drag coefficient in the two-wall channel configuration can be significantly higher than in an unbounded flow. In the case of two-wall channels with the heights equal to several sphere diameters the drag coefficient is significantly higher than that in a single-wall channel for the same distances between the sphere and the wall. This effect diminishes with increasing channel height.

## 4. Conclusions

In this paper a numerical simulation of the drag coefficient for the sphere in the two-wall channel is performed. The flow conditions correspond to the micro-particle motion with the Reynolds number of $10^{-3}$. The validation of the model is carried out in the conditions of an unbounded flow and a single-wall channel. The simulation data of the validation cases were found to be in good agreement with the experiments and approximations given in the literature. The numerical simulation of the drag coefficient of a sphere in a two-wall channel shows a strong dependence of the sphere drag coefficient on the distance between the sphere and the wall. In the case of a channel with the height of the order of the particle diameter the drag coefficient is much higher than that in an unbounded flow and higher than in a single-wall channel with the same distance between the sphere and the wall.

**Acknowledgements**
The research of G.S. Sokolovskii was partially supported by the Program 111-7 of the Physical Sciences Division of the Russian Academy of Sciences.

**References**

[1] A Ashkin and J M Dziedzic 1977 Observation of resonances in the radiation pressure on dielectric spheres *Physical Review Letters* **38** no. 23 p. 1351.
[2] K C Neuman and S M Block 2004 "Optical trapping," *Review of Scientific Instruments* **75**, no. 9, pp. 2787–2809.
[3] K Svoboda and S M Block 1994 Biological Applications of Optical Forces *Annu Rev Biophys Biomol Struct.*
[4] K Dholakia and T Cizmar 2011 Shaping the future of manipulation *Nature Photon*. **5**, pp. 335-342.
[5] M Padgett and R Bowman 2011 Tweezers with a twist *Nature Photon*. **5**, pp. 343-348.
[6] G S Sokolovskii, V V Dudelev, S N Losev, K K Soboleva, A G Deryagin, K A Fedorova, V I Kuchinskii, W Sibbett, E U Rafailov 2014 Bessel beams from semiconductor light sources *Progress in Quantum Electron.* **38**, no.4, pp. 157–188,
[7] G S Sokolovskii, V V Dudelev, S N Losev, A G Deryagin, V I Kuchinskii, W Sibbett, E U Rafailov 2012 Superfocusing of mutimode semiconductor lasers and light-emitting diodes, *Tech. Phys. Lett.* **38**, pp. 402-404.
[8] G S Sokolovskii, V V Dudelev, S N Losev, M Butkus, K K Soboleva, A I Sobolev, A G Deryagin, V I Kuchinskii, W Sibbett, E U Rafailov 2013 Influence of the axicon characteristics and beam quality parameter $M^2$ on the formation of Bessel beams from semiconductor lasers, *Quantum Electron*. **43**, pp. 423-427.
[9] G S Sokolovskii, S A Zolotovskaya, S N Losev, V V Dudelev, A G Deryagin, V I Kuchinskii, W Sibbett, E U Rafailov 2011 High power Bessel beams from EP-VECSELs, *Proc. SPIE* **7919**, p. 79190J.
[10] G S Sokolovskii, V V Dudelev, S N Losev, A G Deryagin, D A Vinokurov, A V Lyutetskii, N A Pikhtin, S O Slipchenko, I S Tarasov, S A Zolotovskaya, E U Rafailov, V I Kuchinskii, W Sibbett 2010 Study of non diffracting light beams from broad stripe edge emitting semiconductor lasers *Tech. Phys. Lett.* **36**, pp. 9-12.
[11] D A Yanson, E U Rafailov, G S Sokolovskii, V I Kuchinskii, A C Bryce, J H Marsh, W Sibbett 2004 Self-focussed distributed Bragg reflector laser diodes *J. of Appl. Phys.* **95**, pp. 1502-1509.
[12] R G Cox and S K Hsu 1977 The lateral migration of solid particles in a laminar flow near a plane *Int. J. Multiphase Flow* **3**, p. 201.
[13] P Vasseur and R G Cox 1977 The lateral migration of spherical particles sedimenting in a stagnant bounded fluid *Journal of Fluid Mechanics* **80**, no. 3, pp. 561–591
[14] L Zeng, S Balachandar, and P Fischer 2005 Wall-induced forces on a rigid sphere at finite Reynolds number *Journal of Fluid Mechanics* **536**, pp. 1–25
[15] L Zeng, F Najjar, S Balachandar, and P Fischer 2009 Forces on a finite-sized particle located close to a wall in a linear shear flow *Physics of Fluids* **21**, no. 3, p. 033302
[16] A Miyamura, S Iwasaki, and T Ishii 1981 Experimental wall correction factors of single solid spheres in triangular and square cylinders, and parallel plates *International Journal of Multiphase Flow* **7**, no. 1, pp. 41–46
[17] H G Weller, G Tabor, H Jasak, C Fureby 1998 A tensorial approach to computational continuum mechanics using object-oriented techniques *Computers in Physics*, **12**, no. 6
[18] R Clift, J R Grace, and M E Weber 1978 Bubbles, Drops, and Particles, Academic, New York
[19] A J Goldman, R G Cox, and H Brenner 1967 Slow viscous motion of a sphere parallel to a plane wall. I. Motion through a quiescent fluid *Chem. Eng. Sci.* **22**, p. 637